ADVANCED HEALTHCARE MATERIALS

Supporting Information

for *Adv. Healthcare Mater.*, DOI: 10.1002/adhm.202100385

Core Cross-Linked Polymeric Micelles for Specific Iron Delivery: Inducing Sterile Inflammation in Macrophages

Tobias A. Bauer, Natalie K. Horvat, Oriana Marques, Sara Chocarro, Christina Mertens, Silvia Colucci, Sascha Schmitt, Luca M. Carrella, Svenja Morsbach, Kaloian Koynov, Federico Fenaroli, Peter Blümler, Michaela Jung, Rocio Sotillo, Matthias W. Hentze, Martina U. Muckenthaler,* Matthias Barz**

Supporting Information

Core Cross-Linked Polymeric Micelles for Specific Iron Delivery: Inducing Sterile Inflammation in Macrophages

Tobias A. Bauer,[‡][a, b] *Natalie K. Horvat,*[‡][c, d, e] *Oriana Marques,*[d, f] *, Sara Chocarro,* [g] *Christina Mertens,*[f] *Silvia Colucci,*[d, f] *Sascha Schmitt,*[h] *Luca M. Carrella,*[b] *Svenja Morsbach,*[h] *Kaloian Koynov,*[h] *Federico Fenaroli,*[i] *Peter Blümler,*[j] *Michaela Jung,*[k] *Rocio Sotillo,* [g]*Matthias W. Hentze,**[c] *Martina U. Muckenthaler,**[d, e, f] *Matthias Barz**[a, b]

[‡] *These authors contributed equally to this work.*

[a] T. A. Bauer, Prof. Dr. M. Barz
Leiden Academic Centre for Drug Research (LACDR), Leiden University, Einsteinweg 55, 2333CC Leiden, The Netherlands.
E-mail: m.barz@lacdr.leidenuniv.nl

[b] T. A. Bauer, Dr. L. M. Carrella, Prof. Dr. M. Barz
Department of Chemistry, Johannes Gutenberg University Mainz, Duesbergweg 10-14, 55128 Mainz, Germany.

[c] N. K. Horvat[◊], Prof. Dr. M. W. Hentze
European Molecular Biology Laboratory (EMBL), [◊]Collaboration for joint PhD degree between EMBL and the Faculty of Biosciences, University of Heidelberg, Meyerhofstr.1, 69117 Heidelberg, Germany.
E-mail: hentze@embl.org

[d] N. K. Horvat, Dr. O. Marques, Dr. C. Mertens, S. Colucci, Prof. Dr. M. U. Muckenthaler
Molecular Medicine Partnership Unit (MMPU), Otto-Meyerhof-Zentrum, Im Neuenheimer Feld 350, 69120 Heidelberg, Germany.

[e] N. K. Horvat, Prof. Dr. M. U. Muckenthaler
Translational Lung Research Center Heidelberg (TLRC), German Center for Lung Research (DZL), University of Heidelberg, Im Neuenheimer Feld 350, 69120 Heidelberg, Germany.

[f] Dr. O. Marques, Dr. C. Mertens, S. Colucci, Prof. Dr. M. U. Muckenthaler
Department of Pediatric Oncology, Hematology, Immunology, and Pulmonology, Heidelberg University Hospital, Im Neuenheimer Feld 350, 69120 Heidelberg, Germany.
E-mail: martina.muckenthaler@med.uni-heidelberg.de

[g] S. Chorcarro, Prof. Dr. R. Sotillo
Department of Thoracic Oncology, German Cancer Research Center (DKFZ), Heidelberg, Im Neuenheimer Feld 280, 69120 Heidelberg, Germany.

[h] S. Schmitt, Dr. K. Koynov, Dr. S. Morsbach
Max Planck Institute for Polymer Research, Ackermannweg 10, 55128 Mainz, Germany.

[i] Dr. F. Fenaroli
Department for Biosciences, University of Oslo, Blindernveien 31, 0371 Oslo, Norway.

[j] Dr. P. Blümler
Institute of Physics, Johannes Gutenberg University Mainz, Staudingerweg 9, 55128 Mainz, Germany.

[k] Dr. Michaela Jung
Institute of Biochemistry I, Faculty of Medicine, Goethe-University Frankfurt, Theodor-Stern-Kai 7, 60590 Frankfurt am Main, Germany.

Table of Contents

Results and Discussion

Polymer Synthesis and Characterization

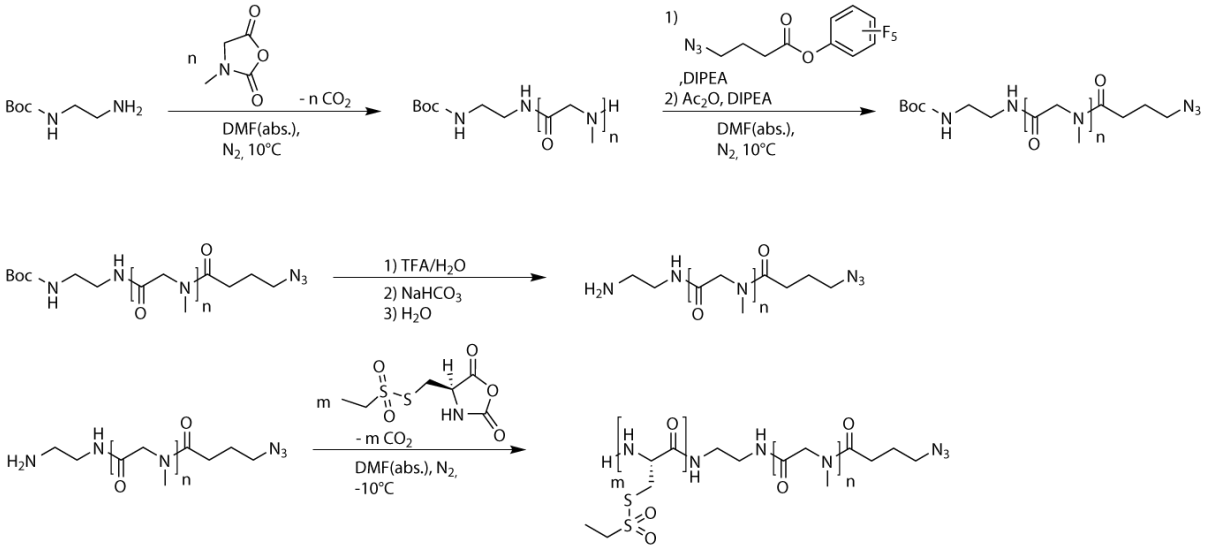

Scheme S1. Polymerization scheme for azide-functionalized $pSar_n$-*block*-$pCys(SO_2Et)_m$ (**P1** to **P3**) copolypepti(o)ides.

Table S1. Characterization of $pSar_n$-*block*-$pCys(SO_2Et)_m$ (**P1** to **P3**) copolymers.

polymer	end-group	X_n pSar[a]	X_n pCys(SO_2Et)[b]	*wt.%* Cys(SO_2Et)	M_n [c]	$Đ$ [c]
P1	Ac	225	31	27.5	31150	2.64
P2	N_3	200	17	18.9	31700	1.25
P3	N_3	170	27	30.4	35100	7.06

[a] HFIP-GPC, relative to pSar standards. [b] as determined by ^{1}H-NMR. [c] HFIP-GPC, relative to PMMA standards.

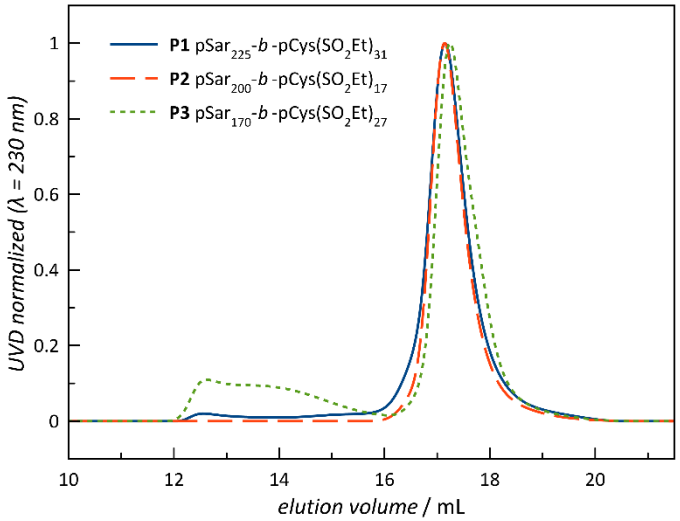

Figure S1. HFIP-GPC traces of **P1-P3** (see Table 1). Note that secondary structures are not suppressed in the eluent (HFIP containing 3 gL^{-1} of CF_3COOK), and elution volumes may be influenced by the degree of secondary structure formation of the $pCys(SO_2Et)_m$ block, as reported by previously.[1–3]

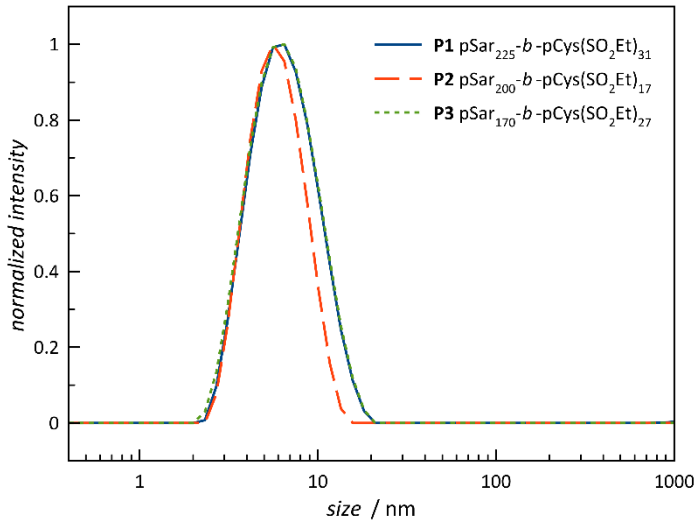

Figure S2. Single-angle DLS of pSar-*b*-pCys(SO_2Et) block copolymers (**P1** - **P3**) in DMSO (β = 18 g L^{-1}) confirms the absence of larger structures but polymer species only.

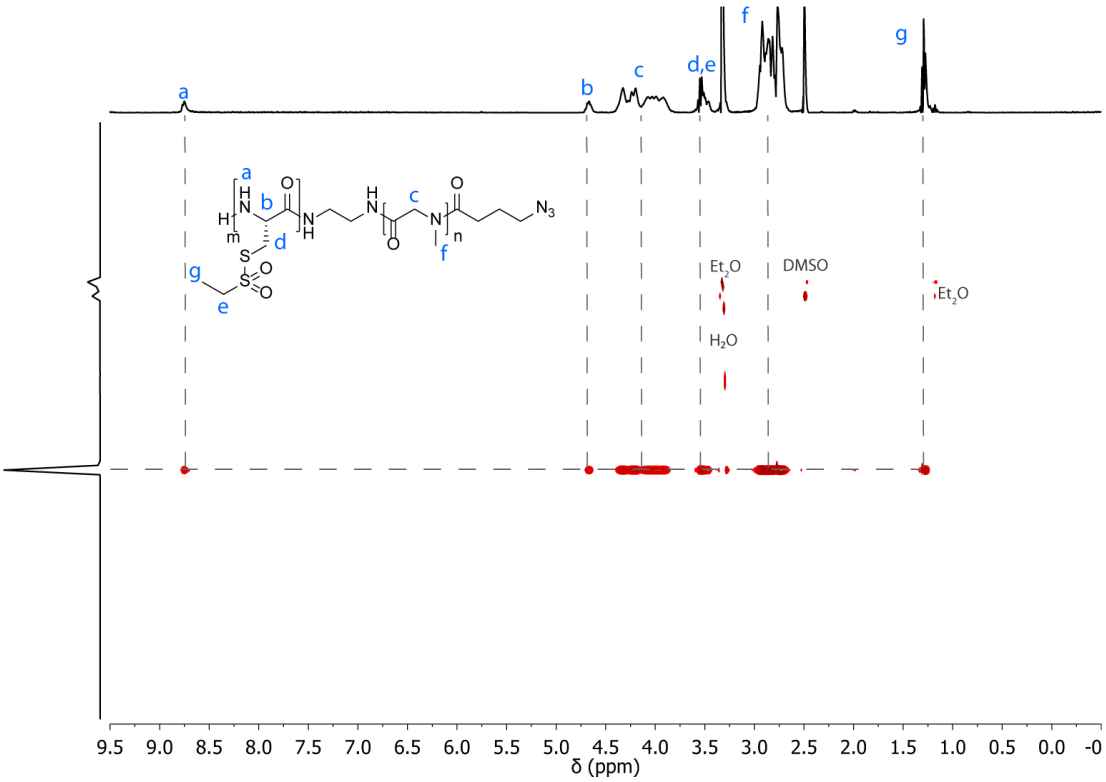

Figure S3. ^{1}H DOSY NMR spectrum of **P1** (pSar$_{225}$-*block*-pCys(SO$_2$Et)$_{31}$) in DMSO-d_6.

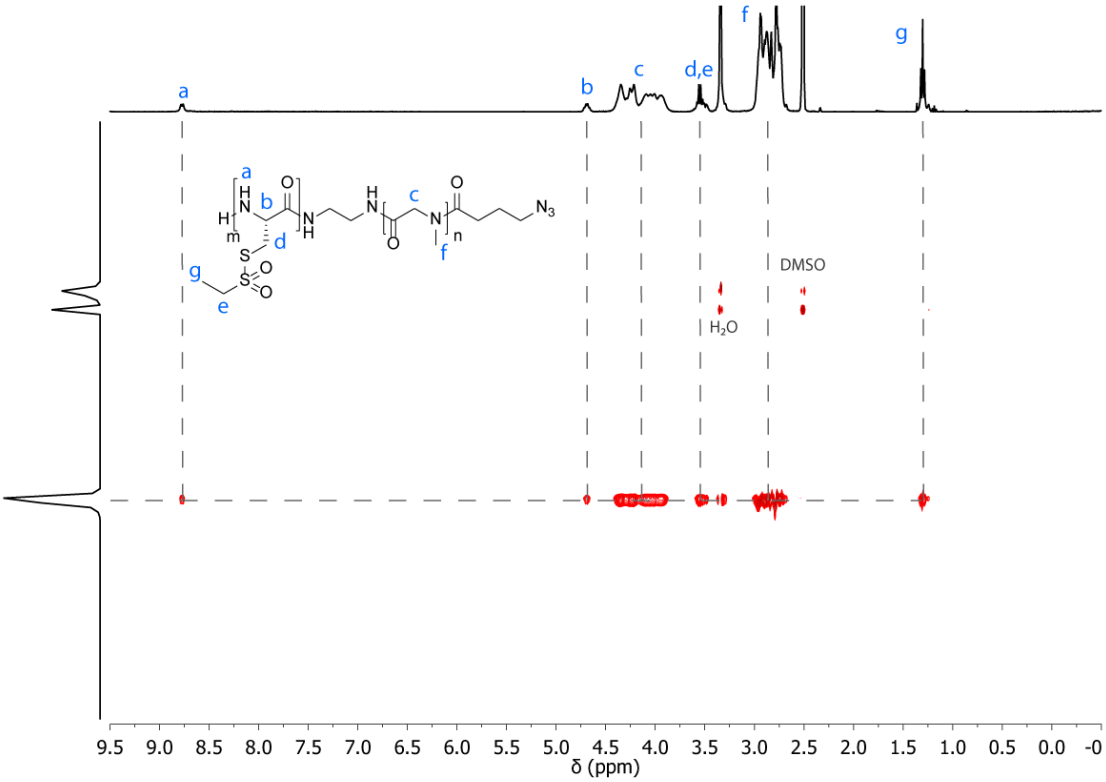

Figure S4. ^{1}H DOSY NMR spectrum of **P2** (pSar$_{200}$-*block*-pCys(SO$_2$Et)$_{17}$) in DMSO-d_6.

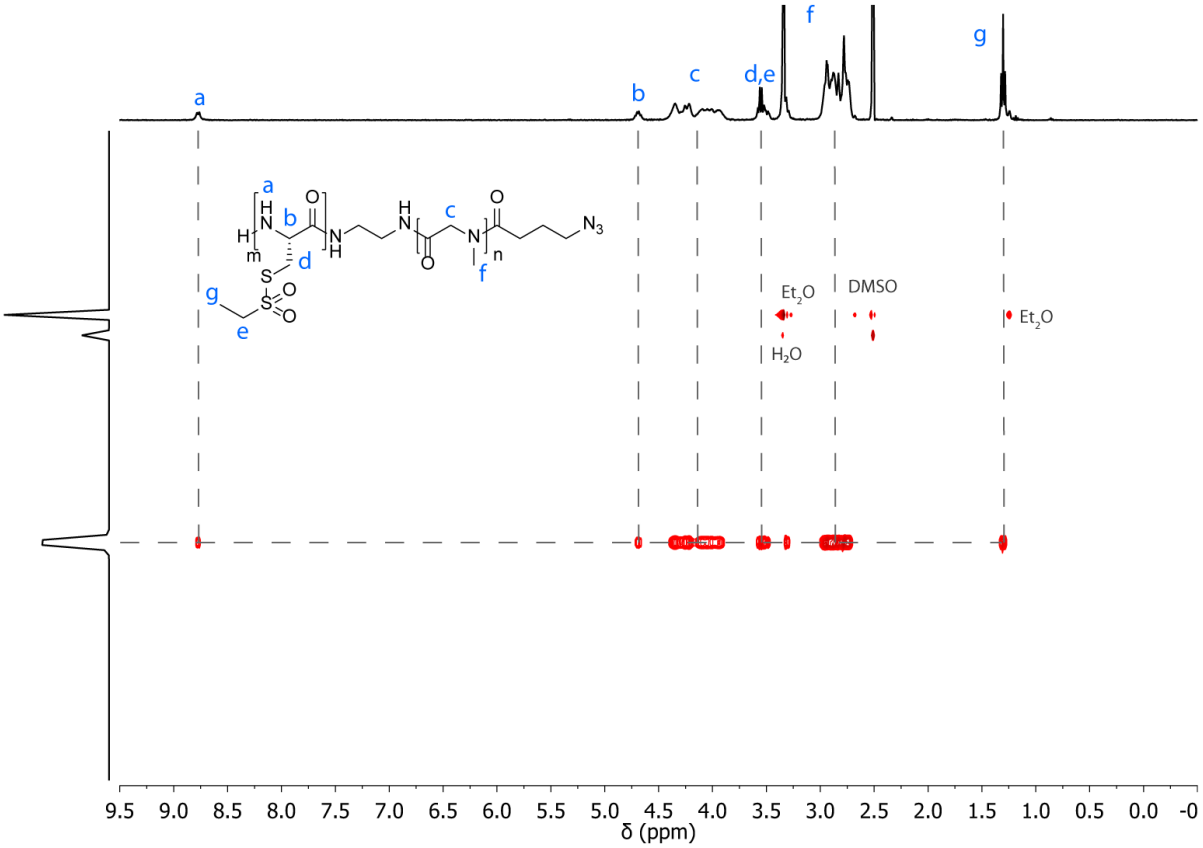

Figure S5. ^{1}H DOSY NMR spectrum of **P3** (pSar$_{170}$-*block*-pCys(SO$_2$Et)$_{27}$) in DMSO-d_6.

Nanoparticle Characterization

Table S2. Characterization of core cross-linked polymeric micelles with and without embedded iron oxide nanoparticles.

particle	polymer	cross-linker	yield	D_h / nm[a]	PDI [a]	*wt.%* Fe_2O_3 [b]	N_{Dye}[c]
SPION-CCPM^{Cy5}	P3	Lipoic acid	22%	82	0.163	33	16.5
SPION-CCPM^{Cy5}#2	P2	Lipoic acid	36%	63	0.122	42	4.1
CCPMs^{Cy5}	P1	*N*-3-Azidopropyl-liponamide	46%	49	0.131	-	2.5

[a] determined by single-angle DLS. [b] Determined by TGA in O_2 atmosphere. [c] Determined by FCS.

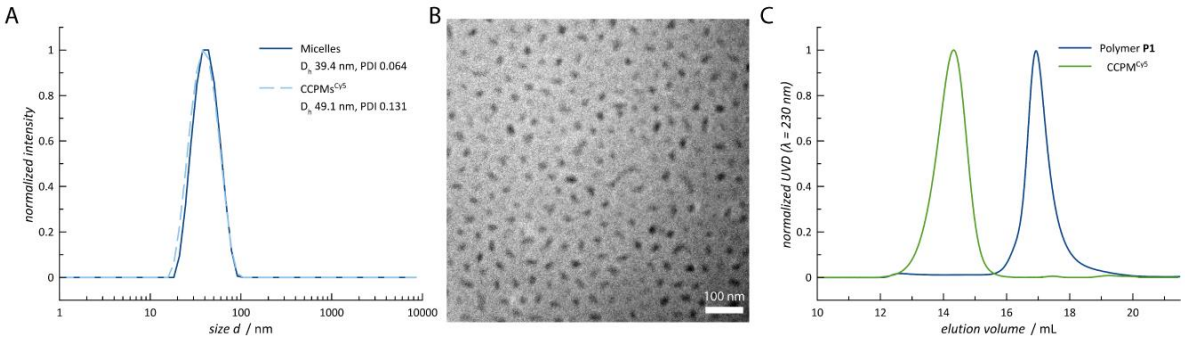

Figure S6. Characterization of CCPM control particles. (A) DLS analysis shows core cross-linked polymeric micelles (CCPMS) with narrow dispersity. (B) CryoTEM confirmed the presence of nanoparticles with sizes well below 100 nm with spherical morphology. (C) HFIP GPC analysis confirmed successful cross-linking.

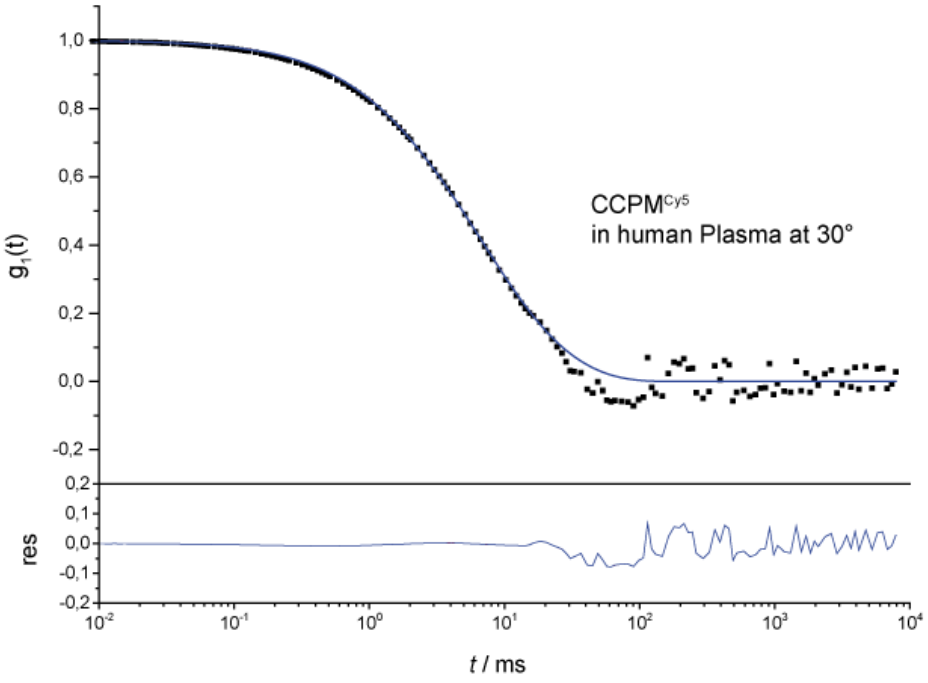

Figure S7. Multi-angle DLS shows no aggregation or increasing sizes for CCPM^{Cy5} after incubation in human plasma.

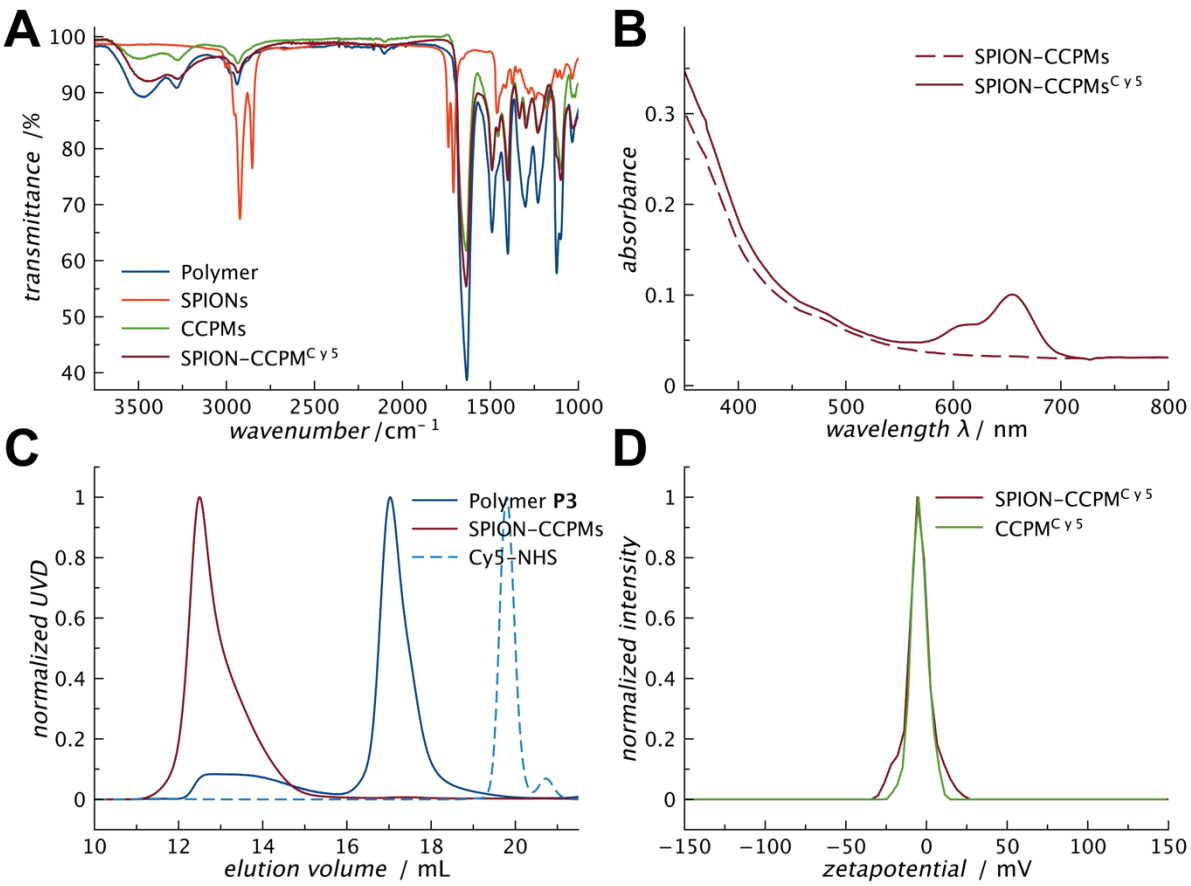

Figure S8. Characterization of SPION-CCPMs (A) ATR-FT-IR Spectroscopy of SPION-CCPMs, CCPMs, SPIONs and block copolymer pSar-*b*-pCys(SO_2Et). (B) UV-Vis spectroscopy of SPION-CCPM dispersions in water. Strong absorbance below λ = 500 nm refers to embedded iron oxide nanoparticles. Distinct absorbance of Cy5 can be detected for SPION-CCPM^{Cy5} after dye conjugation and purification. (C) GPC-analysis in HFIP implies stable cross-linking and absence of residual unconjugated dye or polymer for SPION-CCPM^{Cy5}. The multimodal GPC-trace for polymer P3 is attributed to β-sheet induced aggregation (see Figure S1). (D) Zeta potential distribution. Slightly negative zeta-potentials were determined for both, SPION-CCPM^{Cy5} and CCPM^{Cy5}, in 3 mM sodium chloride solution.

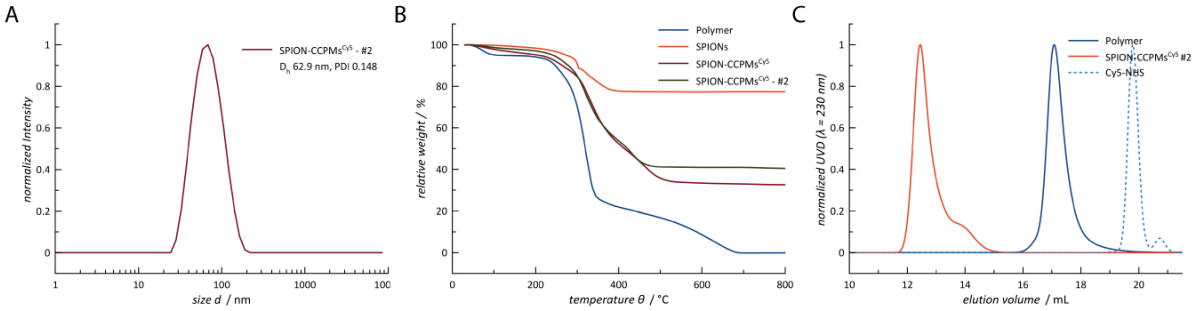

Figure S9. Characterization of SPION-CCPM^{Cy5} #2 particles. (A) DLS analysis reveals SPION-CCPM^{Cy5} #2 particles with narrow dispersity. (B) TGA analysis confirms higher iron oxide contents for SPION-CCPM^{Cy5} #2 (42 wt.%) compared to SPION-CCPM^{Cy5} (33 wt.%). (C) HFIP GPC analysis confirmed successful cross-linking and removal of unconjugated dye or polymer.

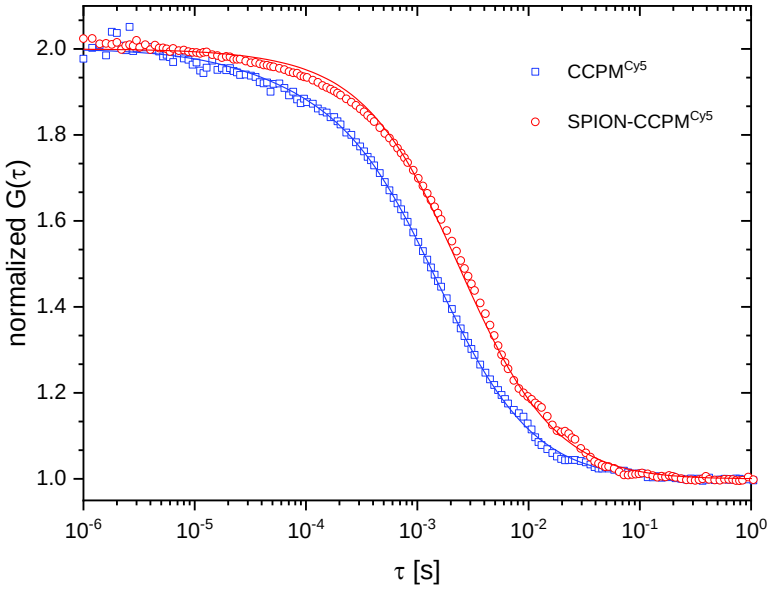

Figure S10. Fluorescence correlation spectroscopy. Normalized autocorrelation curves of Cy5-labelled SPION-CCPMs^{Cy5} (red circles) and CCPMs^{Cy5} (blue squares) measured in PBS buffer. The solid lines represent the corresponding fits with eq. 2 (main text). The fitting was done using single component (*m* = 1 in eq. 2) that confirms the absence of unconjugated dye.

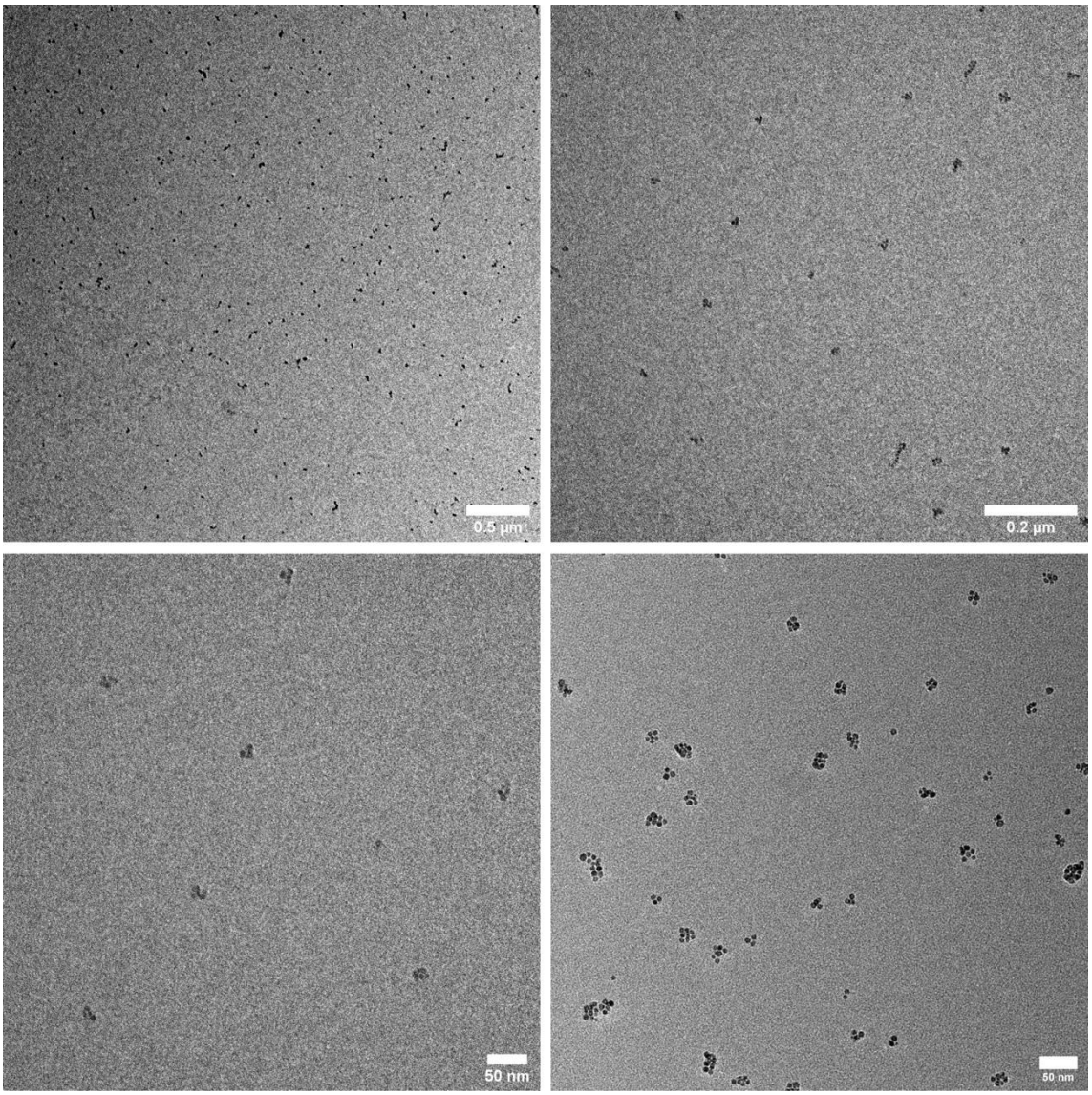

Figure S11. Additional TEM images of SPION-CCPMs^{Cy5}.

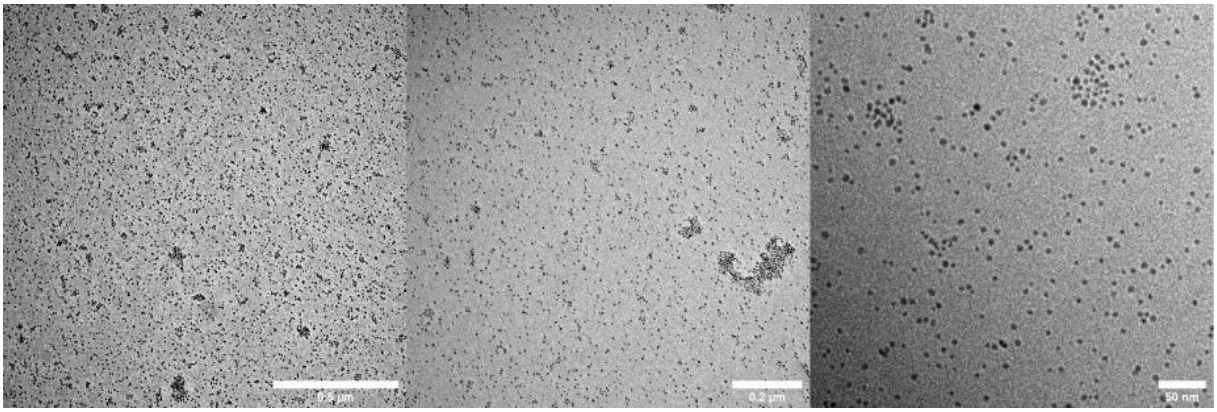

Figure S12. TEM images of oleic acid coated SPIONs. No organized clusters of nanoparticles can be detected.

Magnetic Response & Guidance

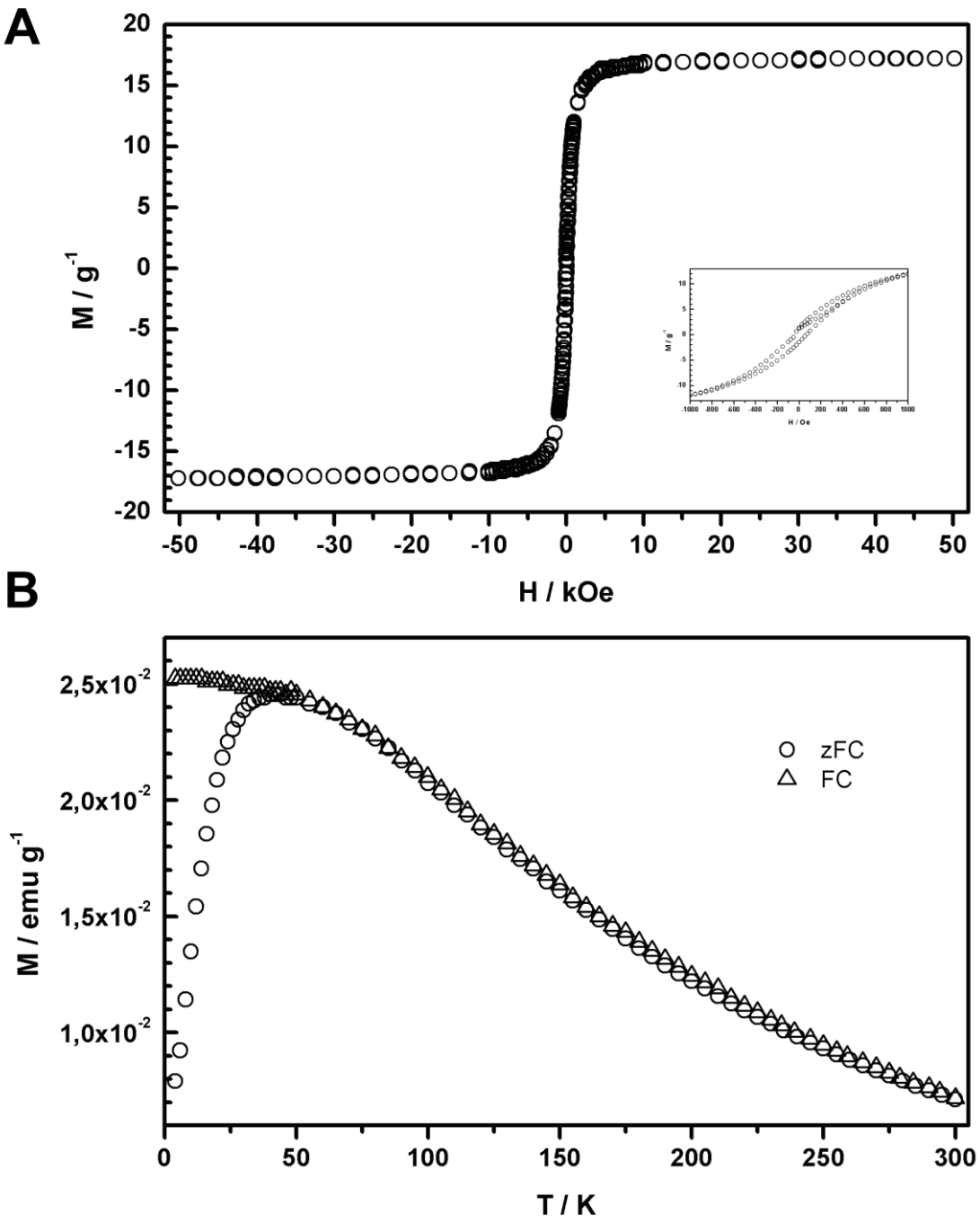

Figure S13. (A) Magnetization hysteresis loop recorded for SPION-CCPMs at 5K conforms superparamagnetic behavior. (B) Zero field cooling/field cooling curves revealed a blocking temperature of 42 K, confirming the presence of superparamagnetic iron oxide nanoparticles.[4]

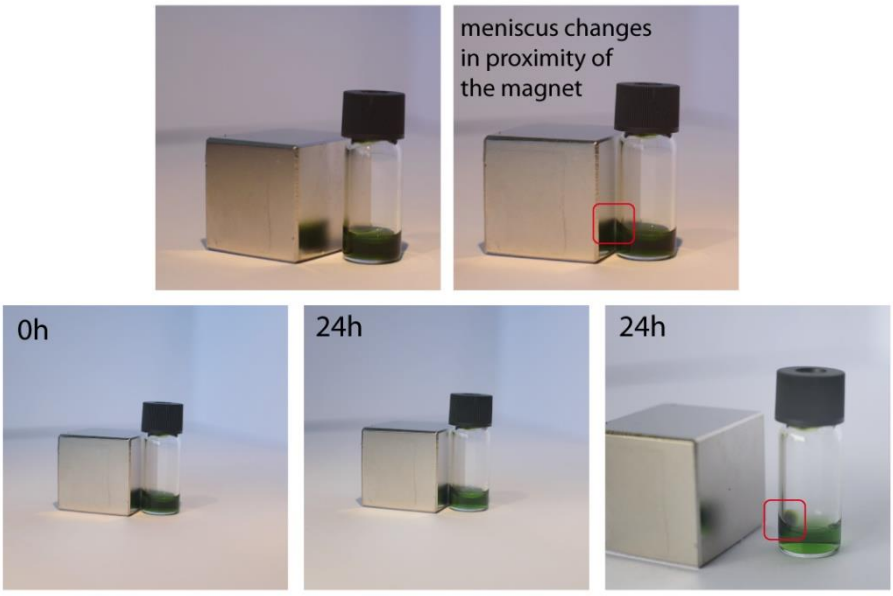

Figure S14. Images of the magnetic response of SPION-CCPM^{Cy5} dispersions in water. (upper images) In proximity of a permanent magnet, the meniscus of the dispersion changes immediately. (lower images) Slow accumulation of SPION-CCPM^{Cy5} by magnetic force.

Figure S15. Image of the quadrupolar/dipolar ring-type magnet used for magnetic guidance experiments.[5]

Magnetic Guidance *in vivo*

If a magnetic particle should be moved against a blood stream, the magnetic force, F_{mag}, must overcome the hydrodynamic (Stokes) friction, F_{fric}. A straight-forward calculation then gives

$$F_{mag} > F_{\mathrm{fric}} \tag{S1}$$

$$mG = \varrho VMG > 6\pi\eta R_h v \tag{S2}$$

Where m [Am^2] is the magnetic moment of the particle and G [$T \cdot m^{-1}$] the magnetic field gradient. It is more useful to express m by a magnetization per mass M [$Am^2 \cdot kg^{-1}$] times its mass or density (ρ [$kg \cdot m^{-3}$]) times particle volume (V [m^3]). On the other side of the equation, the dynamic viscosity, η [Pa·s], of the surrounding liquid, its velocity, v [$m \cdot s^{-1}$], relative to a sphere with hydrodynamic radius, R_h [m], is determining the friction. If, like in our case, a larger particle contains N spherical SPION centers of radius R, this can be rearranged to find the necessary field gradient to counter the blood flow

$$G > \frac{9 \cdot v \cdot \eta \cdot R_h}{2 \cdot \rho \cdot N \cdot R^3 \cdot M} \tag{S3}$$

Equation S3. Approximation of the magnetic gradient required to direct magnetic particles in dispersion of a fluid in motion.

with v as the velocity of the blood flow ($2 \cdot 10^{-3}$ $m \cdot s^{-1}$ (zebrafish embryo)[6], 0.15 $m \cdot s^{-1}$ (human)[7]), η as the dynamic viscosity of the blood ($5 \cdot 10^{-3}$ Pa·s (zebrafish embryo)[6], $3.5 \cdot 10^{-3}$ Pa·s (human)[8]), R_h as the hydrodynamic radius of the SPION-CCPM nanoparticle, ρ as the density of the nanoparticle (approx. 1500 $kg \cdot m^{-3}$ for SPION-CCPMs), R as the radius magnetic SPION core, and M as the saturation magnetization of the SPION nanoparticle (50 $Am^2 \cdot kg^{-1}$ for 10 nm iron oxide nanoparticles, 74 $Am^2 \cdot kg^{-1}$ for magnetite nanoparticles > 20 nm)[4].

For SPION-CCPMs with R_h = 40 nm, each containing 5 SPIONs cores of R = 5 nm, the magnetic gradient needs to be larger than $3.84 \cdot 10^7$ $T \cdot m^{-1}$ or $2.02 \cdot 10^9$ $T \cdot m^{-1}$ to overcome the velocity of the blood flow and guide those nanoparticles in the vasculature of zebrafish embryos or humans. For SPION-CCPMs with increased dimension of the magnetic cores (R_h = 20 nm, R_{SPION} = 10 nm, N = 3) values slightly decrease to $2.70 \cdot 10^6$ $T \cdot m^{-1}$ or $1.42 \cdot 10^8$ $T \cdot m^{-1}$ for zebrafish embryos or humans, still by far extending the capabilities of the displayed magnet guidance system (G = 2.5 $T \cdot m^{-1}$).[5]

Macrophage Uptake & Stimulation

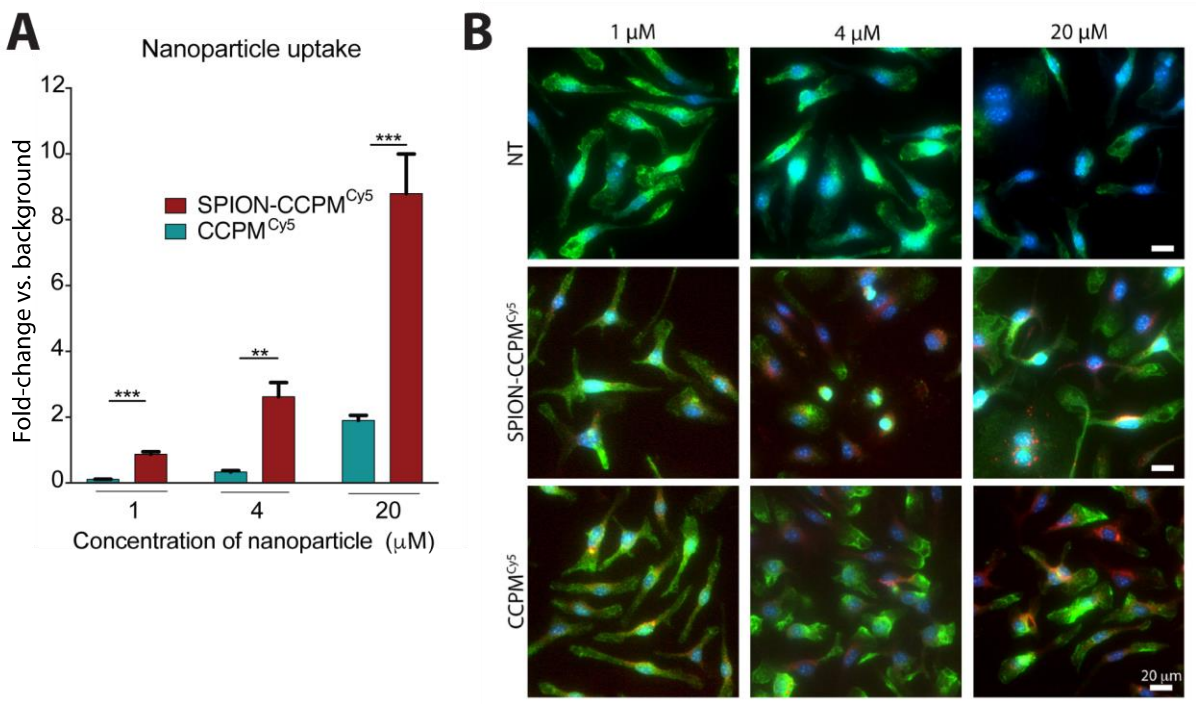

Figure S16. Concentration dependent uptake of SPION-CCPMs^{Cy5} and CCPMs^{Cy5} in BMDMs. (A and B) Non-treated (NT) BMDMs, or BMDMs treated with increasing concentrations of SPION-CCPMs^{Cy5} or CCPMs^{Cy5} (red) for 24 hrs. (A) Internalization of nanoparticles was measured by FACS fluorescence detection (intensity of Cy5). (B) Representative images of BMDMs with and without nanoparticle treatment. Cells were stained with Iba1 (green), a cell surface marker for macrophages, and DAPI. Data reported as mean ± SEM, n = 3 independent experiments. One-way ANOVA (black): * $p < 0.01$, ** $p < 0.001$, *** $p < 0.0001$.

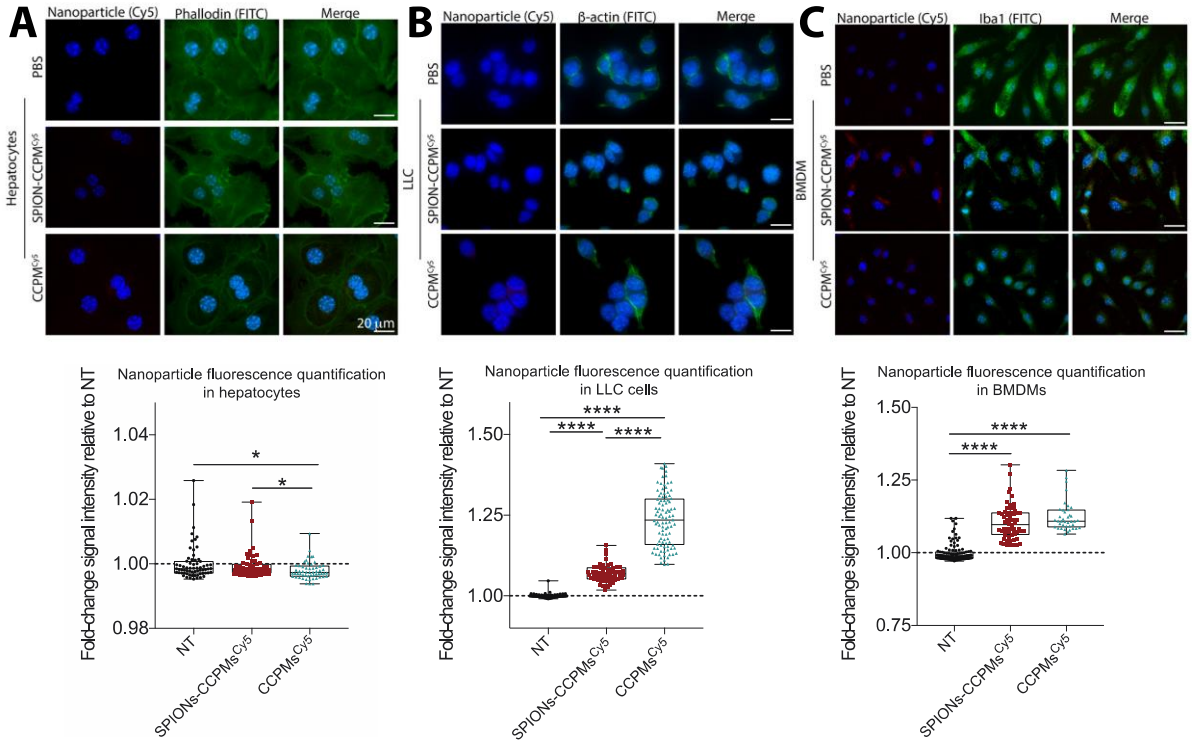

Figure S17. Uptake of SPION-CCPMs and CCPMs in primary murine Hepatocytes, LLCs and BMDMs. Cells were incubated with SPION-CCPMs or CCPMs. Amount of SPION-CCPMs added to cells was calculated based on iron concentration from the core and the amount of CCPMs was calculated to match the mass of CCPMs contained within SPION-CCPMs. (A) Representative images of primary hepatocytes, (B) Lewis Lung Cancer Cells (LLCs), and (C) BMDMs treated with SPION-CCPMsCy5 or CCPMsCy5 (red) for 24 hours. Quantification of nanoparticle signal within cells is below each respective cell type, whereby at least n = 30 cells was analyzed. Primary hepatocytes and LLCs were stained with Phallodin or β-actin (green) and DAPI (blue). BMDMs were stained with Iba1 antibody (green). Data reported as n ± Standard Error of the Mean (SEM). One-way ANOVA: * $p < 0.01$, ** $p < 0.001$, *** $p < 0.0001$.

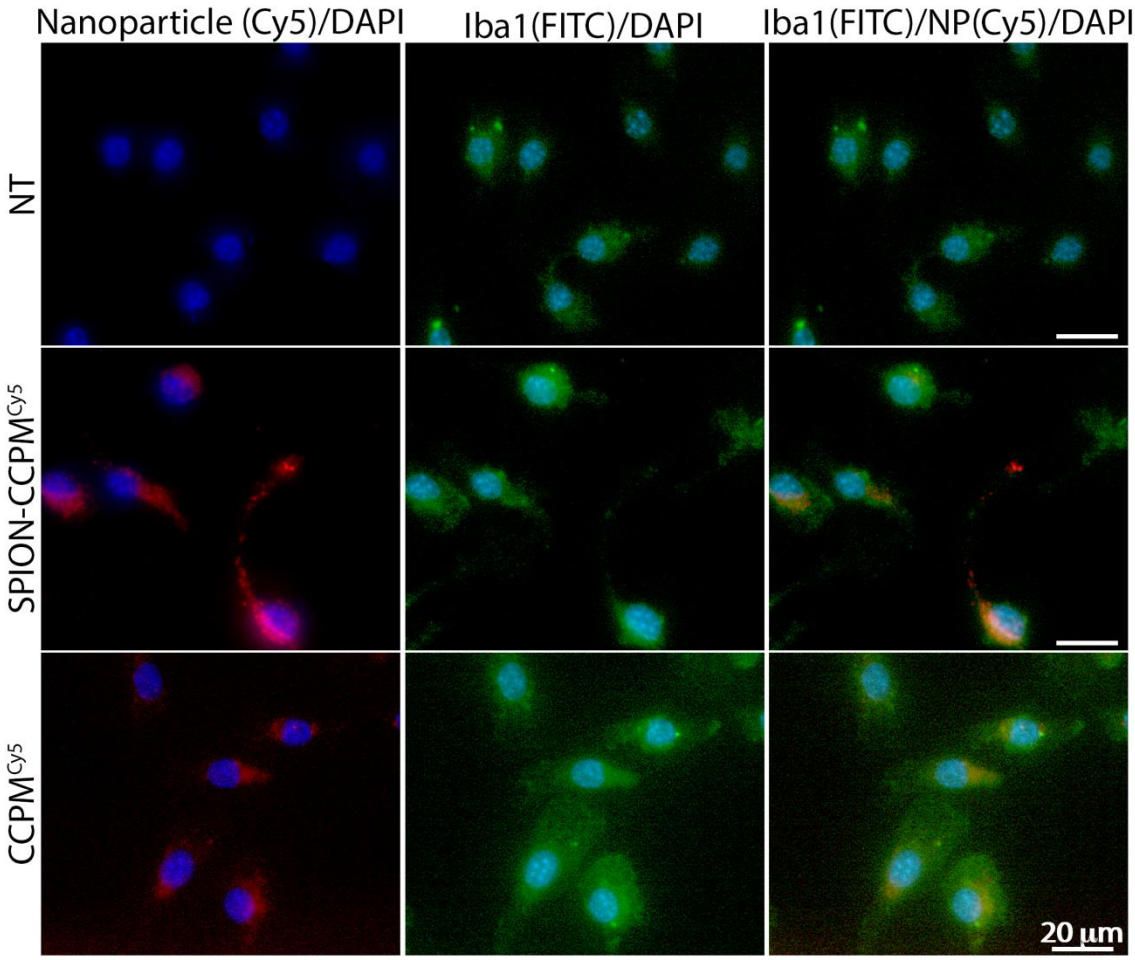

Figure S18. SPION-CCPMs and CCPMs are taken up by BMDMs after a 1-hour incubation. BMDMs were incubated with 20 µM SPION-CCPMs or CCPMs and fixed with 4 % paraformaldehyde after one hour. Cells were stained with a macrophage marker, Iba1 (green), and DAPI (blue).

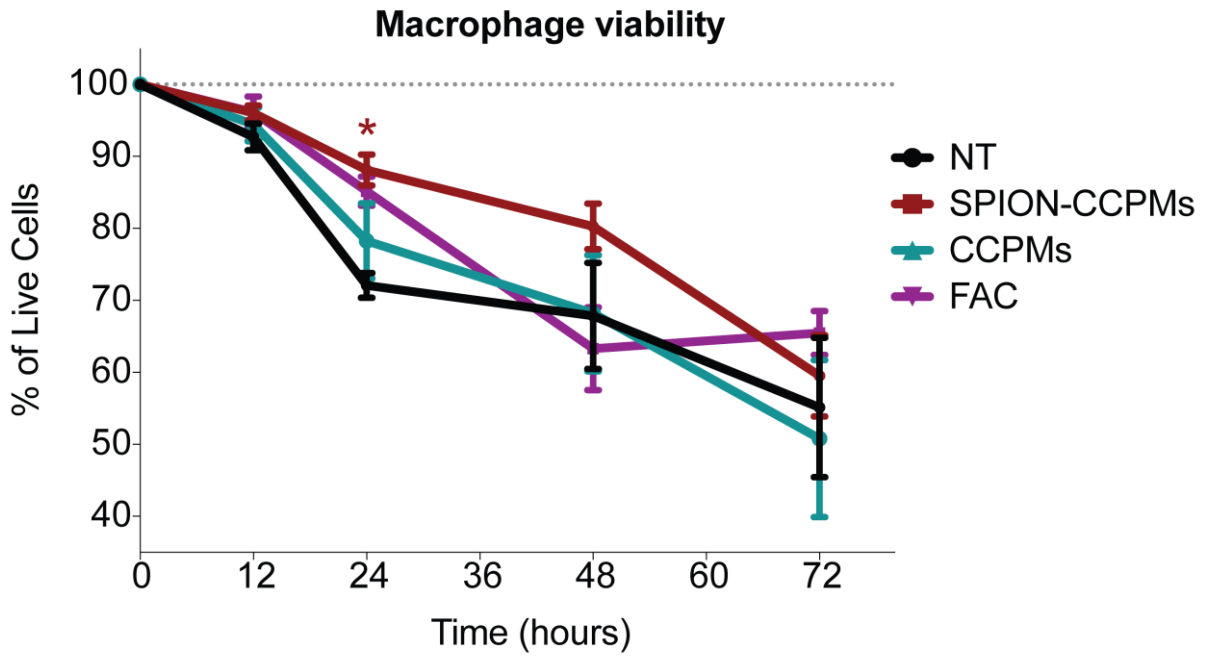

Figure S19. SPION-CCPMs do not cause cytotoxicity in BMDMs. Cells were incubated with 20 μM SPION-CCPMs, dose matched CCPMs, or 20 μM ferric ammonium citrate (FAC). Lactate dehydrogenase (LDH) quantities were measured in the supernatant of cell cultures at 490 nm wavelength after adding CytoTox 96© substrate (Promega). Values are represented as a percentage of the 0 hour condition at each time point. Data reported as n ± SEM. n = 3 independent experiments. One-way ANOVA: * $p < 0.05$, ** $p < 0.01$, *** $p < 0.001$.

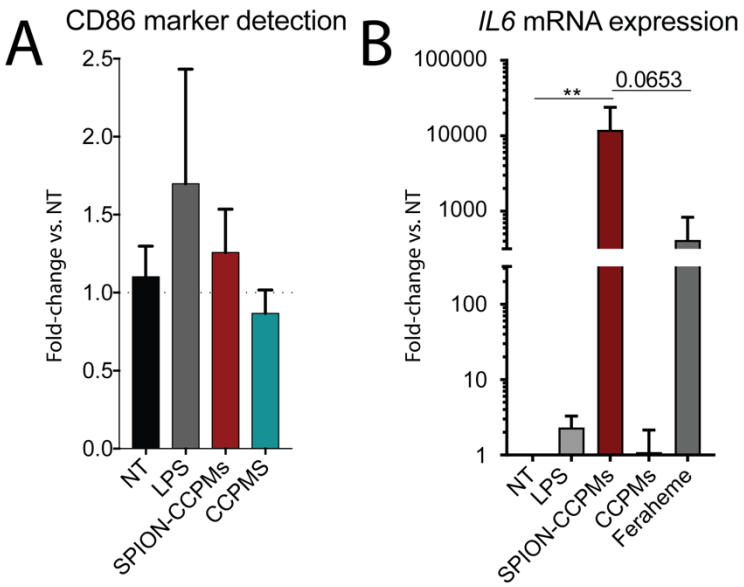

Figure S20. SPION-CCPMs and not CCPMs activate an inflammatory response in human macrophages. (A and B) Human peripheral monocytes were differentiated for 10 days using M-CSF to produce macrophages. Macrophages were incubated with 20 μM SPION-CCPMs, Feraheme, CCPMs, or 100 ng/mL lipopolysaccharide (LPS). After 24 hours, cells were harvested for FACS analysis to detect the cell surface markers CD80 and CD86 (A) or differential cytokine mRNA expression using qPCR (B). (B) Data show mean and SEM of mRNA expression compared to the non-treated (NT) condition and all samples were corrected for *RPL19* mRNA expression. One-way ANOVA (black): * $p < 0.05$, ** $p < 0.01$, *** $p < 0.001$, **** $p < 0.0001$.

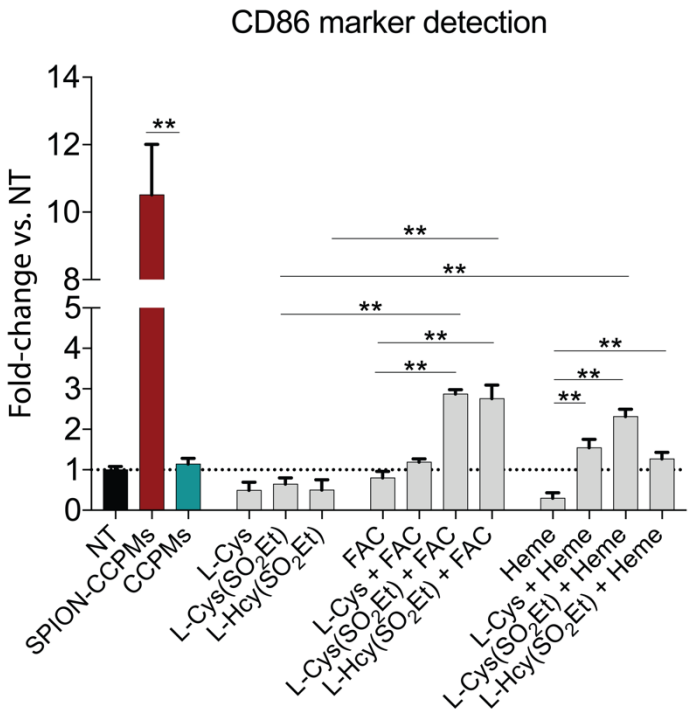

Figure S21. CD86 protein expression in macrophages following treatment with various cysteine dimers. Cells were incubated for 24 hours with 20 µM iron (SPION-CCPMs, heme or ferric ammonium citrate (FAC)), CCPMs, L-cysteine (L-Cys), *S*-ethylsulfonyl-L-cysteine (L-Cys(SO_2Et)), *S*-ethylsulfonyl-L-homocysteine (L-Hcy(SO_2Et)), and cell surface marker CD86 was measured using fluorescence detection by FACS. Values are represented as fold-change compared to non-treated (NT) condition. Data show mean and SEM, n = 2 independent experiments. One-way ANOVA (black): * $p < 0.05$, ** $p < 0.01$, *** $p < 0.001$, **** $p < 0.0001$.

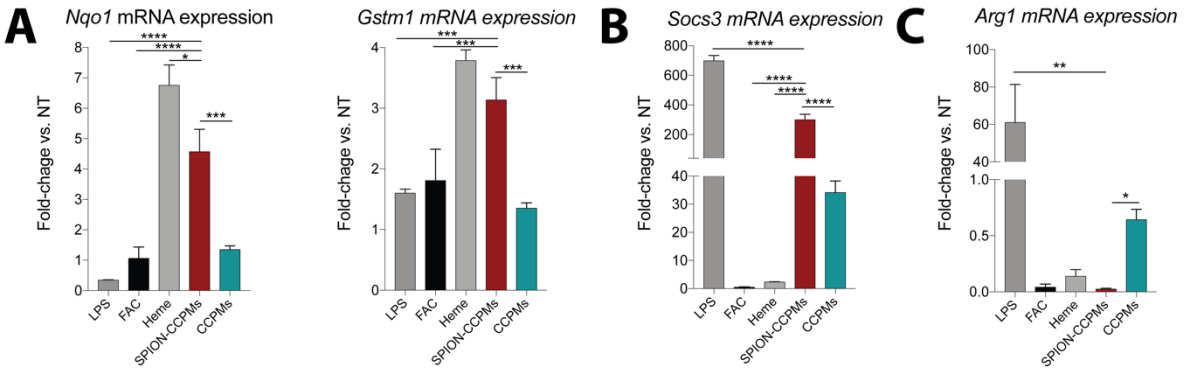

Figure S22. SPION-CCPMs induce sterile inflammation in macrophages. (A-C) BMDMs were incubated with 100 ng/mL LPS, 20 μM FAC, 20 μM Heme, 20 μM SPION-CCPMs or CCPMs for 18 hours. Amount of SPION-CCPMs added to cells was calculated to 20 μM iron from the core and the amount of CCPMs added to cells was calculated to match the mass of CCPMs contained within SPION-CCPMs. The graphs show mean and SEM of mRNA expression compared to the non-treated (NT) condition and all samples were corrected for *Rpl19* mRNA expression. One-way ANOVA (black): * $p < 0.05$, ** $p < 0.01$, *** $p < 0.001$, **** $p < 0.0001$.

Table S3. Antibodies used for Flow Cytometry

Antibody	Fluorophore	Clone	Isotype	Manufacturer
Anti-mouse cell culture experimentation				
CD206	Alexa Fluor 700	MR6F3	Rat IgG2b, κ	ThermoFisher
CD38	FITC	90	Rat IgG2a, κ	BioLegend
CD86	Brilliant Violet 421	GL-1	Rat IgG2a, κ	BioLegend
CD80	Brilliant Violet 650	16-10A1	Armenian Hamster IgG	BioLegend
MHC II	PE-Cy7	M5/114.15.2	Rat IgG2b, κ	BioLegend
Anti-mouse *in vivo* experimentation				
CD45	PerCP-Cy5.5	104	N/A	ThermoFisher
Ly6G	FITC	1A8	N/A	BioLegend
Ly6C	PE-Dazzle	HK1.4	N/A	BioLegend
F4/80	BV605	T45-2342	N/A	ThermoFisher
CD11c	PE	N418	N/A	BioLegend
Siglec-F	APC-Cy7	E50-2440	N/A	ThermoFisher
CD11b	PerCP	ICRF44	N/A	ThermoFisher
CD64	BV711	X54-5/7.1	N/A	BioLegend
CD80	BV650	16-10A1	Armenian Hamster IgG	BioLegend
CD71	BV510	RI7217	Rat IgG2a, κ	BioLegend
MerTK	BV421	108928	Rat IgG2a	ThermoFisher
Anti-human				
CD80	PE	2D10	Mouse IgG1, κ	BioLegend
CD86	Alexa Fluor 488	IT2.2	Mouse IgG2b, κ	BioLegend

Table S4. Primers for quantitative RT-PCR (*mus musculus*)

Gene	Sequence
Arg1	Forward 5' AATCTGCATGGGCAACCTGT 3'
	Reverse 5' GTCTACGTCTCGCAAGCCAA 3'
Cxcl10	Forward 5' ACGTGTTGAGATCATTGCCAC 3'
	Reverse 5' GT CGCACCTCCACATAGCTT 3'
Fpn1	Forward 5' TGTCAGCCTGCTGTTTGCAGGA 3'
	Reverse 5' TCTTGCAGCAACTGTGTCACCG 3'
Gstm1	Forward 5' TCCGTGCAGACATTGTGGAG 3'
	Reverse 5' CTGCTTCTCAAAGTCAGGGTTG 3'
Ho-1	Forward 5' AGGCTAAGACCGCCTTCCT 3'
	Reverse 5' TGTGTTCCTCTGTCAGCATCA 3'
Il6	Forward 5' GCTACCAAACTGGATATAATCAGGA 3'
	Reverse 5' CCAGGTAGCTATGGTACTCCAGAA 3'
Il1β	Forward 5' GCAACTGTTCCTGAACTCAACT 3'
	Reverse 5' ATCTTTTGGGGTCCGTCAACT 3'
Nos2	Forward 5' TGGAGACTGTCCCAGCAATG 3'
	Reverse 5' CAAGGCCAAACACAGCATACC 3'
Nqo1	Forward 5‘ AGCGTTCGGTATTACGATCC 3'
	Reverse 5‘ AGTACAATCAGGGCTCTTCTCG 3'
Rpl19	Forward 5' AGGCATATGGGCATAGGGAAGAG 3'
	Reverse 5' TTGACCTTCAGGTACAGGCTGTG 3'
Slc7a11	Forward 5' TCCACAAGCACACTCCTCTG 3'
	Reverse 5' CGTCAGAGGATGCAAAACAA 3'
Socs3	Forward 5‘ CCTTTGACAAGCGGACTCTC 3'
	Reverse 5‘ GCCAGCATAAAAACCCTTCA 3'
Tfr1	Forward 5' CCCATGACGTTGAATTGAACCT 3'
	Reverse 5' GTAGTCTCCACGAGCGGAATA 3'
Tnfα	Forward 5' TGCCTATGTCTCAGCCTCTTC 3'
	Reverse 5' GAGGCCATTTGGGAACTTCT 3'

Table S5. Primers for quantitative RT-PCR (*homo sapiens*)

Gene	Sequence
IL6	Forward 5' AAATTCGGTACATCCTCGACGGA 3'
	Reverse 5' GGAAGGTTCAGGTTGTTTTCTGC 3'
IL1β	Forward 5' CTCGCCAGTGAAATGATGGCT 3'
	Reverse 5' GTCGGAGATTCGTAGCTGGAT 3'
RPL19	Forward 5' TCGCCTCTAGTGTGTCCTCCG 3'
	Reverse 5' GCGGCCCAAGGTGTTTTTC 3'
TNFα	Forward 5' ATGAGCACTGAAAGCATGATCC 3'
	Reverse 5' GAGGGCTGATTAGAGAGAGGTC 3'

References

[1] O. Schäfer, D. Huesmann, M. Barz, *Macromolecules* **2016**, *49*, 8146.

[2] D. Huesmann, A. Birke, K. Klinker, S. Türk, H. J. Räder, M. Barz, *Macromolecules* **2014**, *47*, 928.

[3] T. A. Bauer, C. Muhl, D. Schollmeyer, M. Barz, *Macromol. Rapid Commun.* **2020**, 2000470.

[4] A. Demortière, P. Panissod, B. P. Pichon, G. Pourroy, D. Guillon, B. Donnio, S. Bégin-Colin, *Nanoscale* **2011**, *3*, 225.

[5] O. Baun, P. Blümler, *J. Magn. Magn. Mater.* **2017**, *439*, 294.

[6] C. Y. Chen, M. J. Patrick, P. Corti, W. Kowalski, B. L. Roman, K. Pekkan, *Biorheology* **2011**, *48*, 305.

[7] R. F. Schmidt, F. Lang, M. Heckmann, *Physiologie Des Menschen*, **2010**.

[8] R. Brandes, R. Busse, in *Physiol. Des Menschen*, **2010**, p. 576f.

Appendix

^{1}H NMR Spectra

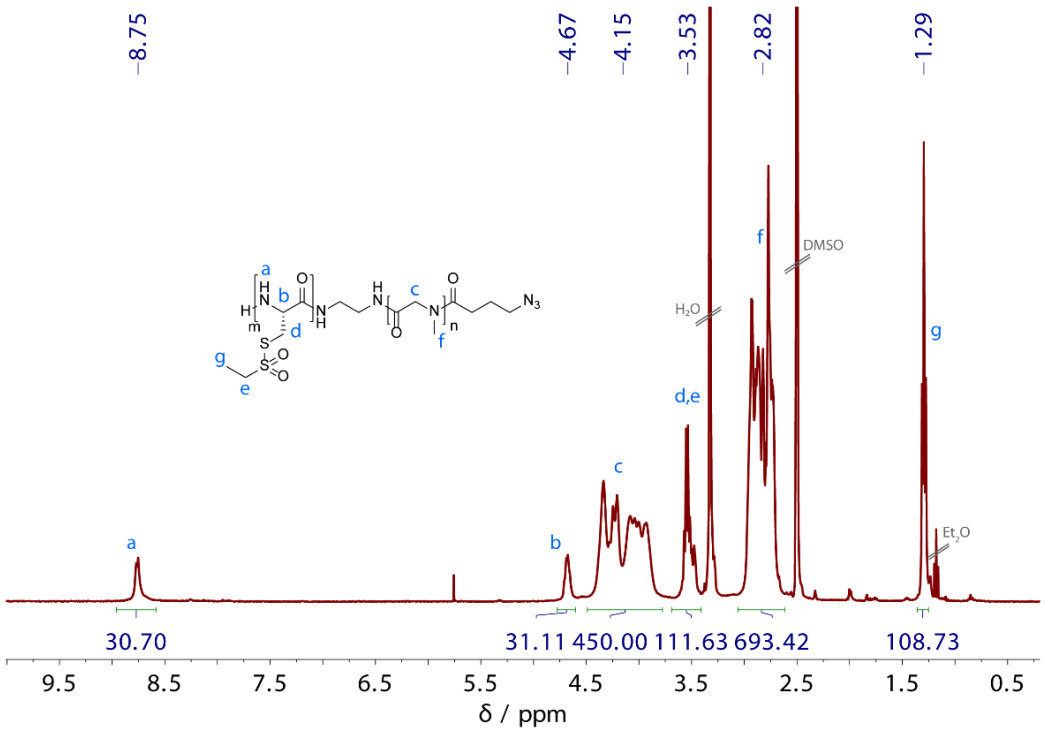

Figure S23. ^{1}H NMR spectrum of **P1** ($pSar_{225}$-*block*-$pCys(SO_2Et)_{31}$) in DMSO-d_6.

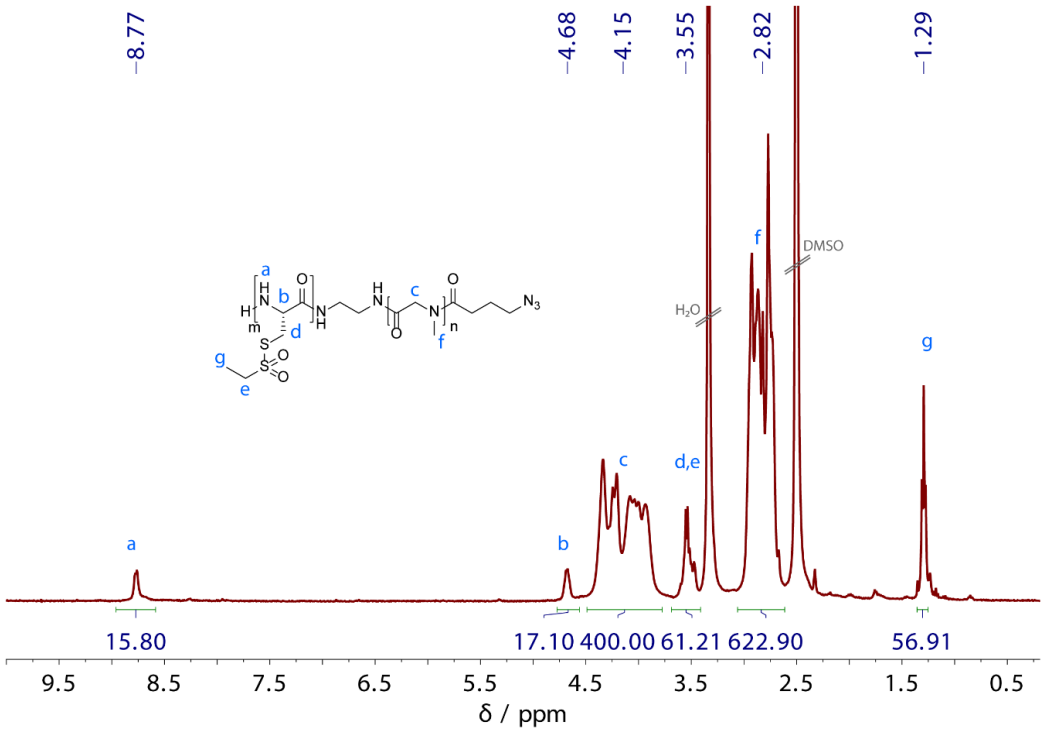

Figure S24. ^{1}H NMR spectrum of **P2** (pSar$_{200}$-*block*-pCys(SO$_2$Et)$_{17}$) in DMSO-d_6.

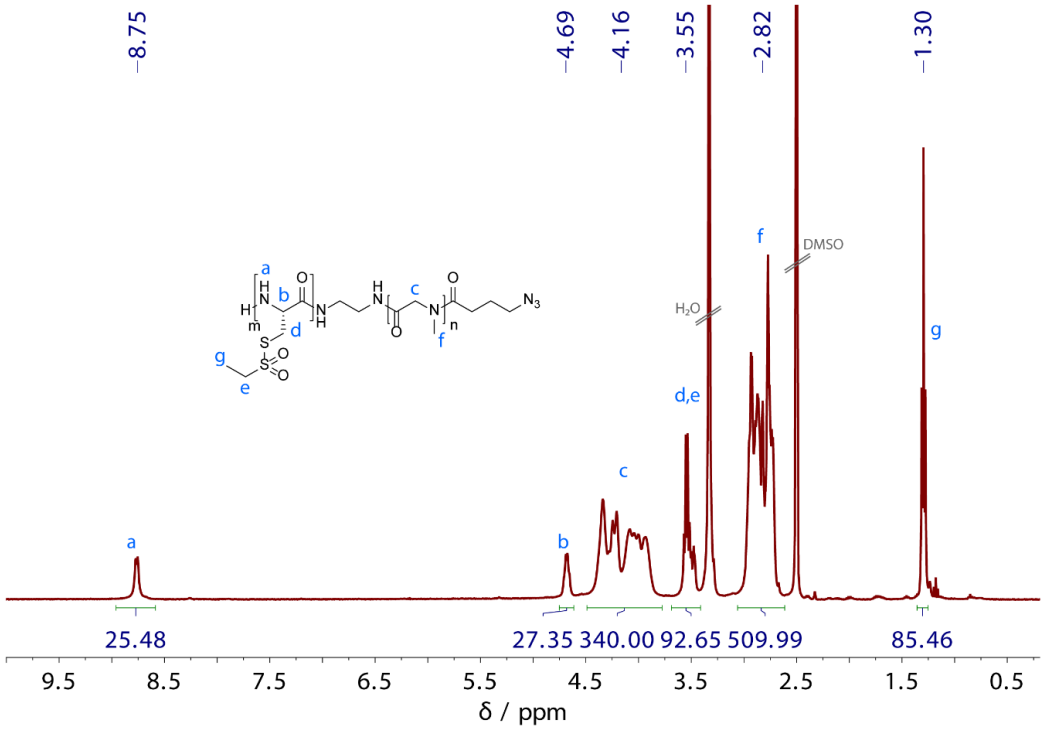

Figure S25. ^{1}H NMR spectrum of **P3** (pSar$_{170}$-*block*-pCys(SO$_2$Et)$_{27}$) in DMSO-d_6.

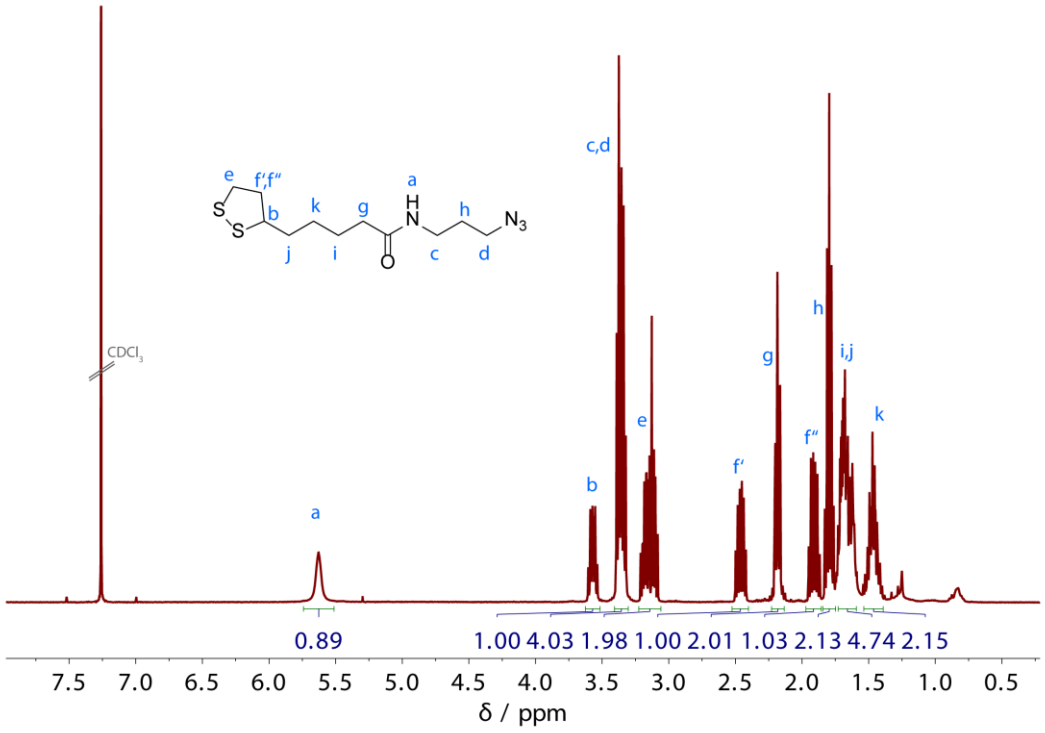

Figure S26. ^{1}H NMR spectrum *N*-3-azidopropyl liponamide in $CDCl_3$.